Cavities for light and sound: a cavity-enhanced platform for quantum acoustics

Fisicaro, M.

3 Investigation of spurious bulk acoustic waves in surface acoustic wave devices by acoustic fringe analysis

Full characterization of surface acoustic wave (SAW) devices is not trivial. We use an optical Michelson interferometer with spatial scanning capabilities, to characterize GHz SAW cavities on GaAs, and we analyze the acoustic field maps by 2-dimensional Fourier analysis of the acoustic interference fringes. While our experimental setup allows for simultaneous measurement of the amplitude and phase of the acoustic field, we show that amplitude-only measurements are sufficient to detect secondary effects such as the presence of spurious bulk acoustic waves. This is possible due to the interference of bulk waves with the surface waves, which leads to an acoustic-wavelength spatial periodicity in the amplitude of the acoustic field, distinct from the half-wavelength spatial periodicity of standing SAWs. By spatial Fourier filtering the images of the acoustic field, we are able to separate the distribution of surface and bulk waves across the SAW cavities, and to detect imperfections and impurities on the surface of the device.

This chapter is in preparation for submission: M. Fisicaro, T. A. Steenbergen, Y.C. Doedes and W. Löffler, Investigation of spurious bulk acoustic waves in surface acoustic wave devices by acoustic fringe analysis.

3.1 Introduction

High-frequency acoustic waves in solids are widely used in modern technologies: with a phase velocity 10^5 times smaller than the electromagnetic counterpart, acoustic waves have a shorter wavelength, in the order of μm at GHz frequencies, enabling miniaturization of signal-processing devices such as RF electronic filters [7, 8, 94, 95]. Depending on the specific type of acoustic waves employed, these devices can be separated in bulk acoustic wave (BAW) and surface acoustic wave (SAW) devices, based on the propagation of the acoustic waves in the bulk or surface of the material.

In recent years, high-frequency acoustic waves also became of interest in the field of quantum technology and research, due to their ability to couple to a variety of different quantum systems [20–25, 29, 69, 70]. Here SAWs have particular importance due to their intrinsic surface confinement, which allows them to travel long distances with little dissipation, enabling quantum protocols relying on itinerant phonons [38–40]. The coupling between phonons and quantum systems on the other hand relies on localized phonons, due to the enhanced interaction provided by the phonon confinement [29].

For this reason, among SAW devices, cavities are of great importance, and even though cavities with high quality factors have been demonstrated at cryogenic temperatures [23, 24, 96], their realization with a small mode volume has only recently been achieved [20, 28, 52, 97, 98]. For this purpose, all loss mechanism must be reduced, such as diffraction losses, material losses, and BAW scattering losses [29, 48–50]. The latter in particular poses a problem in the realization of high-Q, small mode-volume SAW cavities, and even if there are approaches to mitigate these losses, they can not always be avoided [29, 99, 100]. Excitation of spurious BAWs in SAW devices is a very well known problem, but its investigation is primarily done by means of all-electrical measurements [49, 50, 99, 101–103]. There are a few reports of direct observation of BAWs in SAW devices with optical probes, but only measuring the bottom or the side of the substrate [104, 105].

Here we report the observation of spurious BAWs in SAW devices, by optically imaging the out-of-plane displacement on the top surface of SAW cavity devices. This is easily possible with a setup that allows for simultaneous measurement of amplitude and phase of the acoustic field, but we show that amplitude-only measurements are sufficient to identify the presence of spurious BAWs. This is because the interference of bulk and surface waves, leads to an acoustic-wavelength spatial periodicity in the amplitude of the acoustic field, distinct from the half-wavelength spatial periodicity originating from standing SAWs.

We investigate GHz SAW cavities on (001)-cut GaAs, by using a Michelson interferometer with spatial scanning capabilities, to image the amplitude of the out-of-plane surface displacement across the whole device, obtaining an image of the distribution of the acoustic field. By using 2D Fourier analysis and filtering, we are able to separate the spatial distribution of the spurious bulk waves, from that of the surface waves, and to detect imperfection and impurities on the surface of the device. Furthermore, on top of the Rayleigh waves propagating along the [011] direction of the GaAs substrate, the analysis of the 2D Fourier transform also revealed the presence of pseudo (or leaky) surface waves along other directions, which are Rayleigh waves coupled to a transverse horizontal bulk wave [106–108], most likely originating from diffraction of the Rayleigh waves or scattering from impurities on the GaAs surface.

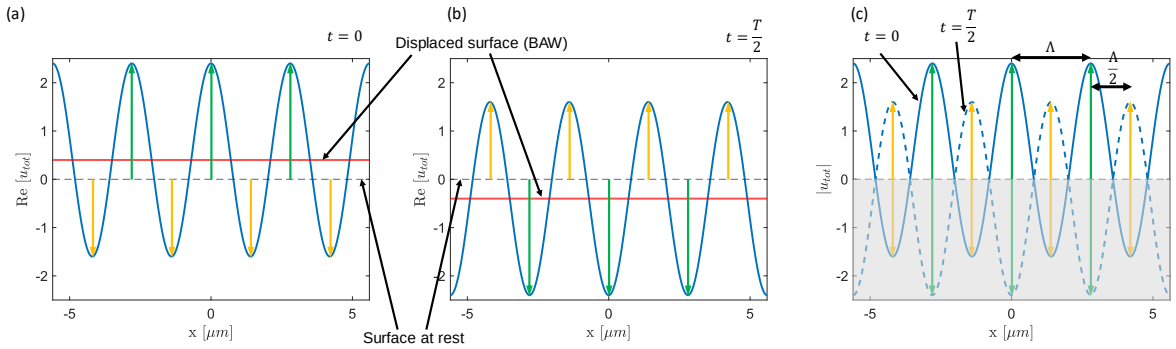

Figure 3.1: Interference of standing SAWs with BAWs. (a) Plot of the out-of-plane total displacement ($\mathrm{Re}[u_{tot}]$) at time $t = 0$: the red line indicates the displaced surface caused by the BAW, and the blue line indicates the standing SAWs displacement, with respect to the displaced surface. The green (yellow) arrows indicate the distances of the oscillating surface from its rest position, showing an enhanced (decreased) displacement for the portion of the standing wave that is moving in phase (out of phase) with the bulk wave. (b) Plot of the out-of-plane total displacement ($\mathrm{Re}[u_{tot}]$) at time $t = T/2$, corresponding to half oscillation. (c) Total surface oscillation at time $t = 0$ (full blue line), and at time $t = T/2$ (dashed blue line). The combination of these two lines in the non-shaded area, correspond to the absolute value of the total out-of-plane surface displacement. The green (yellow) arrows show the portion of the standing wave where the surface displacement is amplified due to constructive (destructive) interference between the surface standing wave and the bulk wave, leading to a Λ-periodic modulation of the surface displacement. All plots are based on Eqs. 3.4, 3.5 with parameters $u_L = u_R = 1$, $u_B = 0.2$, $\varphi_L = \varphi_R = \varphi_B = 0$, $g(x) = 1$, and SAW wavelength $\Lambda = 2.8\,\mu$m.

3.2 Interference of surface and bulk waves

We first study the combined surface displacement of surface and bulk acoustic waves: first we show how by measuring the complex displacement (amplitude and phase), we can easily separate SAWs and BAWs, then we show how, due to the interference of surface and bulk waves, an amplitude-only measurement is sufficient to identify the presence of spurious BAWs in a SAW device.

Let us start by considering the out of plane displacement generated by a combination of left and right traveling SAWs:

$$\begin{aligned} u_{left} &= u_L e^{i(Kx+\Omega t)} e^{i\varphi_L} \\ u_{right} &= u_R e^{i(-Kx+\Omega t)} e^{i\varphi_R} \ , \end{aligned} \tag{3.1}$$

where u_L (u_R) is the out-of-plane displacement amplitude, φ_L (φ_R) a generic phase term, $\Omega = 2\pi/T$ the angular frequency of the SAW, where T is the oscillation period, $K = 2\pi/\Lambda$ the wavenumber with Λ the SAW wavelength, and x is the direction along which the surface waves are excited. For the bulk waves, we assume that their amplitude is localized in a specific region of space and we write the out-of-plane displacement as

$$u_{bulk} = u_B g(x) e^{i\Omega t} e^{i\varphi_B} \ , \tag{3.2}$$

where u_B is the peak out-of-plane displacement amplitude, $g(x)$ is a continuous, non-diverging, non-periodic and slowly varying function of x, with values in the interval $g(x) \in [0, 1]$. The total out-of-plane displacement is given by

$$u_{tot}(x) = u_{left} + u_{right} + u_{bulk} \tag{3.3}$$

$$= e^{i\Omega t}\left[u_L e^{i(Kx+\varphi_L)} + u_R e^{i(-Kx+\varphi_R)} + u_B g(x) e^{-i\varphi_B}\right] . \tag{3.4}$$

Since the total displacement is a linear combination of the individual displacements of the different waves, and since the Fourier transform is a linear operation, the spatial Fourier transform of the demodulated total complex displacement at the frequency $f = \Omega/2\pi$ will show three peaks: a peak at the spatial frequency $f_x = 0$, corresponding to the bulk waves, a peak at spatial frequency $f_x = K/2\pi = 1/\Lambda$, corresponding to left-traveling SAWs, and a peak at spatial frequency $f_x = -1/\Lambda$, corresponding to right-traveling SAWs. This means that knowledge of the amplitude and phase of the total surface displacement, allows for the separation of SAWs and BAWs contributions. We now show that, to some extent, this is still possible with an amplitude-only measurement of the total surface displacement. The absolute value of the total out-of-plane displacement is $|u_{tot}(x)| = \sqrt{|u_{tot}(x)|^2} = \sqrt{u_{tot} \times u_{tot}^*}$, and can be written as

$$\begin{aligned} |u_{tot}(x)| &= \sqrt{|u|^2_{DC} + |u|^2_{\Lambda/2} + |u|^2_{\Lambda}} \\ |u|^2_{DC} &= u_L^2 + u_R^2 + u_B^2 g^2(x) \\ |u|^2_{\Lambda/2} &= 2u_L u_R \cos(2Kx + \varphi_L - \varphi_R) \\ |u|^2_{\Lambda} &= 2u_B g(x)\left[u_L \cos(Kx + \varphi_L - \varphi_B) + u_R \cos(Kx - \varphi_R + \varphi_B)\right] . \end{aligned} \tag{3.5}$$

In the equation above we have split the absolute value into three terms: a DC-term with spatial frequency $f_x \sim 0$, a $\Lambda/2$-term with spatial frequency $f_x = 2K/2\pi = 2/\Lambda$, and a Λ-term with spatial frequency $f_x = K/2\pi = 1/\Lambda$. The DC term $|u|^2_{DC}$ denotes the non-periodic term: depending on the particular function $g(x)$, this term is not necessarily constant in x, but can slowly vary. The DC-term is present whenever there is at least one of the displacement components of Eqs. 3.1 and 3.2. The $\Lambda/2$-term $|u|^2_{\Lambda/2}$ represents the usual standing wave pattern given by the interference of a left and right traveling SAWs, and shows a periodicity in x equal to $\Lambda/2$, which is the distance between two adjacent nodes or antinodes. The Λ-term $|u|^2_{\Lambda}$ is a Λ-periodic modulation caused by the interference between left/right traveling waves and the bulk waves, and it is an unequivocal sign of the presence of bulk acoustic waves. The operation of taking the absolute value therefore has the effect of mixing the DC spatial frequency of the complex BAW displacement with the spatial frequencies $f_x = \pm 1/\Lambda$ of the traveling SAWs, leading to the appearance of the two BAWs sidebands in the displacement amplitude, at frequencies $f_x = \pm 1/\Lambda$.

Eq. 3.5 is very generic, and depending on the choice of the parameters u_L, u_R, u_B, φ_L, φ_R, φ_B, $g(x)$ it describes different situations. Let's briefly investigate some of these cases by assuming $\varphi_L = \varphi_R = \varphi_B = 0$, and $g(x) = 1$. For pure BAWs, or traveling SAWs, only one of the amplitudes $u_L, u_{R,} u_B$ is different than zero, resulting in a pure DC-component. For pure standing SAWs, $u_L = u_R$ and $u_B = 0$, resulting only in a $\Lambda/2$-component. For pure right (left) traveling SAWs interfering with BAWs, $u_L = 0$ ($u_R = 0$) and $u_B \neq 0$, resulting in a DC-term and a Λ-term. Finally for standing SAWs interfering with BAWs, we have $u_L = u_R$, $u_B \neq 0$, resulting in $\Lambda/2$ periodic standing wave pattern, where the height of the antinodes is modulated with a spatial periodicity of Λ. This effect is visible because some portions of the standing SAW are in phase with the BAW, and some other

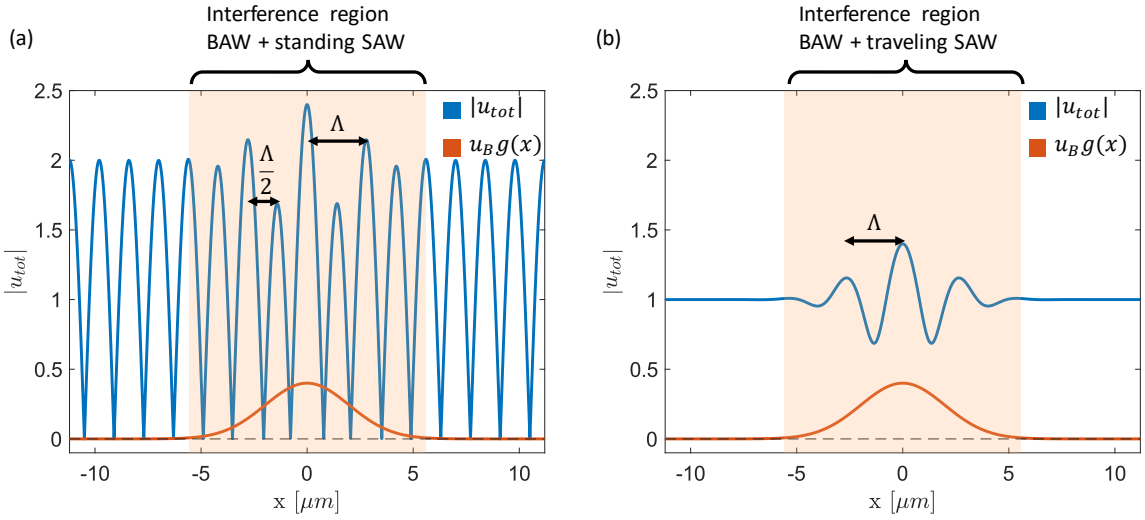

Figure 3.2: Localized SAW-BAW interference. Here we show the effect of introducing localization in Eq. 3.5: as an example we choose $g(x) = \exp(-x^2/\Lambda^2)$, where $\Lambda = 2.8\,\mu$m is the SAW wavelength. (a) shows the interference between standing surface waves ($u_L = u_R = 1$) and bulk waves ($u_B = 0.4$). (b) shows the interference between traveling surface waves ($u_L = 0$, $u_R = 1$) and bulk waves ($u_B = 0.4$). In both (a) and (b), all phases are set to zero ($\varphi_L = \varphi_L = \varphi_B = 0$).

portions are out of phase, leading to constructive or destructive interference, as shown in Fig. 3.1. This is not true anymore if we re-introduce the phase terms, with $\varphi_L = \varphi_R$ and $\varphi_B = \varphi_R + (m+1)\pi/2$, where m is an integer: in this situation the bulk wave has a $\pi/2$ phase shift with respect to the standing surface wave, and even if both waves are present, there is no interference and therefore no Λ-term in the amplitude of the out-of-plane displacement.

Normally, in surface acoustic wave devices, spurious bulk waves are not excited uniformly along the whole device, but originate from localized scatterers which scatter SAWs into bulk waves. In our mathematical model, this is taken into account by the function $g(x)$ that determines the spatial profile of the out-of-plane surface displacement caused by the bulk wave. In Fig. 3.2 we show the localization of the surface-bulk wave interference for a bulk wave with Gaussian surface-profile $g(x) = \exp(-x^2/\Lambda^2)$, both for standing (a) and traveling (b) surface waves, representing the interference pattern that we expect to see for a scatterer with size of the order of the acoustic SAW wavelength Λ.

3.3 Acoustic fringe analysis

Now we validate the model introduced above by investigating the BAW-SAW interference in surface acoustic wave cavities. First we measure the acoustic field distribution across the device, and by Fourier analysis and filtering of the Λ-periodic spatial component, we are able to identify the presence of BAWs, and locate the region of the SAW device where the BAWs are excited.

In particular we investigate two planar SAW cavities with identical configurations, but different cavity lengths, metal thickness and composition. These cavities have been nanofabricated via e-beam lithography and e-beam evaporation of aluminium on a (001)-cut GaAs substrate. Both cavities consist of an IDT with 10 metal finger pairs, and two

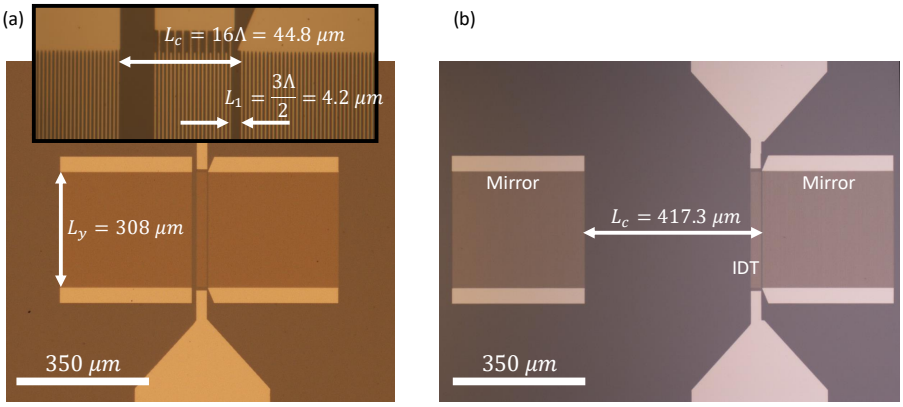

Figure 3.3: Optical microscope images of the short (a) and long (b) cavities. The geometrical cavity length L_c of the short cavity is a multiple integer of $\Lambda/2$, where Λ is the acoustic wavelength at which the cavity is designed to operate. This condition is not satisfied for the long cavity.

metal-grating acoustic mirrors with 250 metal fingers each, with a center-to-center finger spacing of $p = 1.4\,\mu$m, and finger width of $d = 700\,$nm. The length of the fingers on the transverse direction is $L_y = 308\,\mu$m, and the two cavities are both oriented along the [110] direction, for which the speed of the Rayleigh wave is $v_{SAW} \simeq 2860\,$m/s, resulting in an acoustic wavelength $\Lambda \simeq 2.8\,\mu$m at the design frequency $f_{SAW} \simeq 1.02\,$GHz.

The two cavities have different geometrical cavity length of $L_c = 471.3\,\mu$m for the long cavity, and $L_c = 16\Lambda = 44.8\,\mu$m for the short cavity. These distances are measured between the centers of the first metal fingers of the 2 mirrors, and while for the short cavity it is a multiple integer of $\Lambda/2$, this is not true for the long cavity. The distance between the IDT and the adjacent mirror is $L_1 = 3\Lambda/2 = 4.2\,\mu$m for both cavities, also measured between the centers of the metal fingers. For the short cavity we evaporated a 10 nm adhesion layer of Ti, followed by 80 nm of Al, and finally another 10 nm of Ti, for a total metal height of $h = 100\,$nm. For the long cavity we only evaporated $h = 50\,$nm of Al, without any adhesion or top layer; the absence of these two layers does not affect the operation of the cavity. Fig. 3.3 shows microscope pictures of the short (a) and long (b) SAW cavities used in this experiment.

Using the optical scanning Michelson interferometer described in detail in the previous chapter, we image the acoustic field distribution in both the long and short cavities, and we now analyze these measurements by means of 2D Fourier analysis.

3.3.1 Long SAW cavity

We drive the IDT at the resonant frequency of the SAW cavity $f_0 = 1.021965\,$GHz and we image the acoustic field distribution. In Fig. 3.4 (a) we show the amplitude of the out-of-plane displacement. In the left inset we show a cross section of the measurement in the middle of the cavity, where standing waves are visible, with antinodes equally spaced at a distance of $\Lambda/2$. In the right inset we show a cross section of the acoustic field inside the mirror. Next to the exponential decay, we observe also a modulation in the height of the antinodes, with a spatial periodicity of Λ, as predicted by our model.

In Fig. 3.4 (b) we show the 2D Fourier transform of the amplitude of the out-of-plane displacement measured in (a). On the f_x axis, we observe two peaks at the spatial frequencies $f_x = 1/\Lambda = 0.357\,\mu\text{m}^{-1}$ and $f_x = 2/\Lambda = 0.714\,\mu\text{m}^{-1}$, corresponding to a Λ

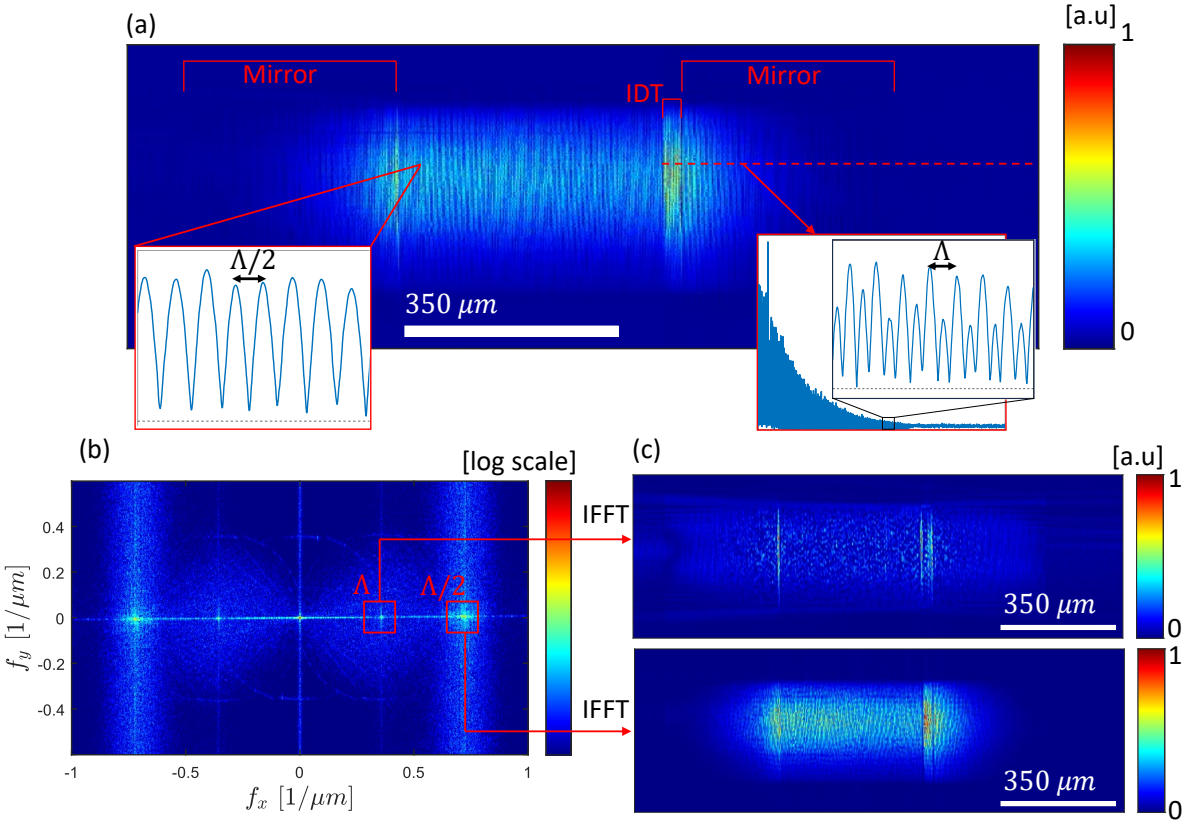

Figure 3.4: Acoustic field distribution in the long cavity. (a) Image of the SAW cavity, showing the amplitude of the out-of-plane displacement. The inset on the left shows a cross section of the standing wave field inside the cavity. The inset on the right shows a cross section of the exponentially decaying field inside the acoustic mirror, where the standing wave pattern is now modulated in amplitude by the BAWs. (b) 2D Fourier transform of (a), showing two peaks at the spatial frequencies $f_x = 0.357\,\mu\text{m}^{-1}$ and $f_x = 0.714\,\mu\text{m}^{-1}$, corresponding to a Λ and $\Lambda/2$ periodicity in the real space. (c) Fourier filtered images obtained from (b) by selecting only the Λ-term (top image) and the $\Lambda/2-$term (bottom image) in the Fourier spectrum.

and $\Lambda/2$ periodicity in real space. There is also a DC term, which is caused partially by spurious BAWs and partially by the presence of spurious traveling SAWs, resulting from the finite reflectivity of the SAW mirrors. Finally we note that the Fourier transform shown here is limited to the spatial frequency range $f_x = [-1, 1]\,\mu\text{m}^{-1}$, and that there are other peaks along the f_x axis at higher spatial frequencies, corresponding to the harmonics of $f_x = 2/\Lambda$, since we are analyzing here the amplitude of the out-of-plane displacement $|u_{tot}(x)| = \sqrt{|u_{tot}(x)|^2}$.

In the 2D Fourier transform, we select the peaks corresponding to the spatial frequencies $f_x = \pm 1/\Lambda$ by applying two narrow square box functions as a mask, and we compute the inverse 2D Fourier transform, obtaining a real-space image of the spatial distribution of the Λ-periodic term. The top image in fig. 3.4 (c) shows the result of this process, while the bottom image shows the spatial distribution of the $\Lambda/2$-periodic term, resulting from Fourier filtering the $f_x = 2/\Lambda$ spatial frequency. While the latter strongly resembles the original image (a), the Λ-periodic component shows high amplitude in the SAW cavity, at

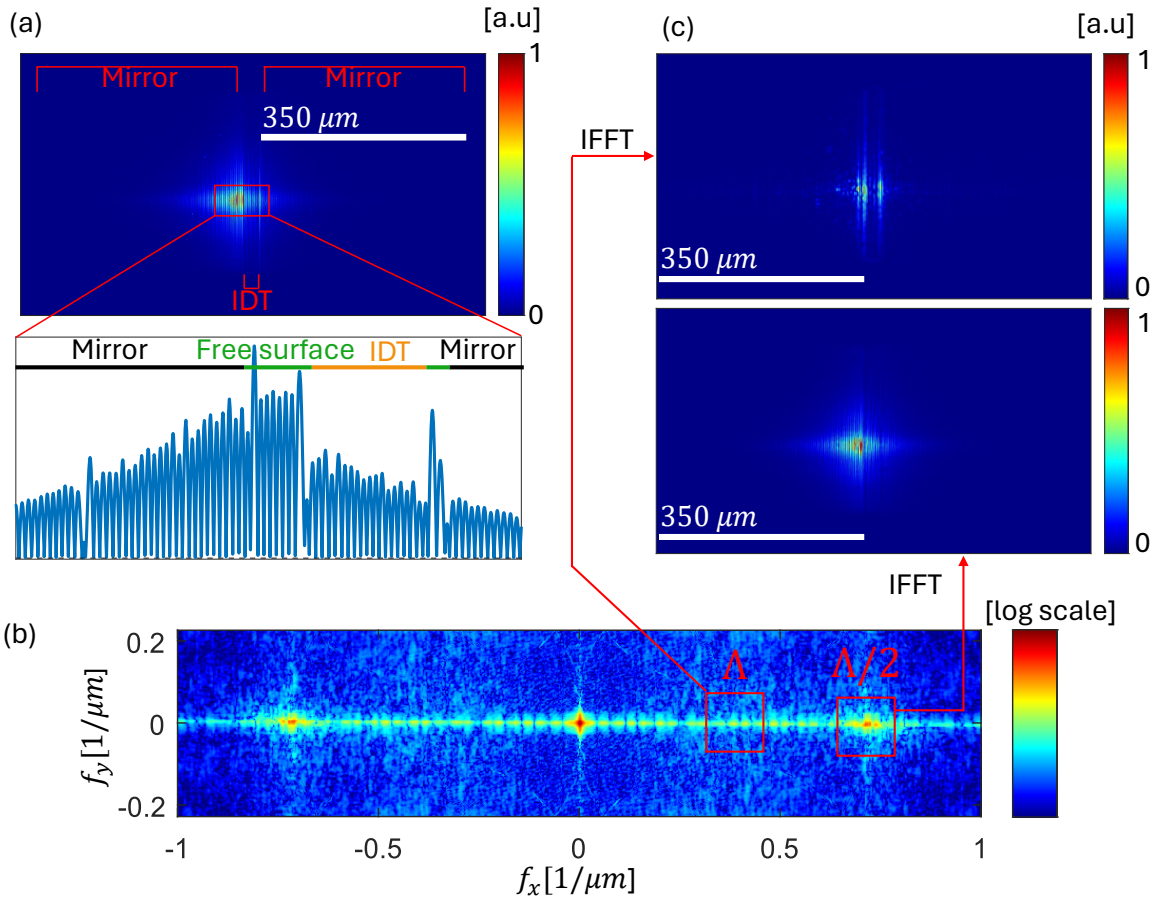

Figure 3.5: Acoustic field distribution in the short cavity, when driven at its resonance frequency. (a) Amplitude of the out-of-plane displacement. In the inset we show the cross section of the acoustic field in the middle of the cavity. We indicate in black the position of the mirrors, in green the position of the free GaAs surface, and in yellow the position of the IDT. (b) 2D Fourier transform of (a), where the peak corresponding to the $\Lambda/2$ term is visible, while there is no visible peak corresponding to the Λ-term. Fourier filtered images obtained from (b) by selecting only the Λ-term (top image) and the $\Lambda/2$-term (bottom image) in the Fourier spectrum.

the line boundaries between free GaAs and the metal grating of the mirrors and IDT. In addition to this, there are several high-amplitude spots, and a low-amplitude background across the whole SAW cavity.

3.3.2 Short SAW cavity

The resonance frequency of the short cavity is found to be $f_0 = 1.0107\,\text{GHz}$. We drive the IDT at this frequency and we measure the amplitude of the out-of-plane displacement, as shown in Fig. 3.5 (a). In the inset we show a cross section in the middle of the cavity. The asymmetry in the amplitude of the field in the left and right mirror is most likely to be attributed to the small gap between the IDT and the right mirror, but a rigorous analysis of this requires a TMM (transfer matrix method) calculation of the field in the Bragg grating.

In Fig. 3.5 (b) we show the 2D Fourier transform of the surface displacement, where now

the peak corresponding to the Λ-component is not visible. Nevertheless, as described for the long cavity, we Fourier filter the spatial frequencies corresponding to the Λ-periodicity and to the Λ/2-periodicity, and we show the result in Fig. 3.5 (c). The results are similar to the long cavity, where the spatial distribution of the Λ/2-component mirrors the non-filtered surface displacement. The Λ-component, however, only shows as bright lines inside the SAW cavity, in correspondence of the interfaces between free surface and metal structures.

As a final experiment, we drive the short SAW cavity at the frequency $f = 0.995\,\mathrm{GHz}$, which is outside of the stopband of the mirrors. The idea is that in this situation the surface acoustic waves are mainly not confined in the cavity, but traveling.

In Fig. 3.6 (a) we show the image of the measured surface displacement (top), and a cross section (bottom) taken at the transverse position indicated by the dashed line. Now the presence of the traveling waves is clear as indicated by the significant DC offset in regions (i) and (iv), corresponding to the free surface outside of the cavity. The regions (ii) and (iii), corresponding to the mirrors, IDT and cavity, show the presence of a spurious resonant mode. This is a weak resonance, as visible by the strong DC component, and most likely appears because we are driving at a sideband of the Bragg mirror. The amplitude asymmetry between the left and right side of the cavity is probably connected to the small gap between the IDT and the right mirror. Fig. 3.6 (b) shows the 2D Fourier transform, where now the peak corresponding to the Λ-periodicity is clearly visible.

In Fig. 3.6 (c) we show the Fourier-filtered images, showing the spatial distribution of the Λ-component (top) and Λ/2-component (bottom). Off-resonance, the surface waves travel through the mirrors almost unaffected, and this shows in the filtered image, where the Λ-component now has bright lines at all the interface between metal and free-surface, also the ones outside of the cavity. BAW scattered from point-like centers are now also visible, and, across the whole device, a faint Λ-component indicates the presence of BAW interfering with traveling surface waves.

3.3.3 Discussion

We now first discuss the images corresponding to the Fourier-filtered Λ-component in Figs. 3.4,3.5,3.6 (c): all of them show strong signals at the interfaces between metal structures and free GaAs surface. This is explained by the theory of SAW reflection by a periodic grating: upon incidence of a SAW on a periodic structure, the single elements of the grating not only reflect the surface waves, but also scatter them into bulk acoustic waves.

In our case the cavity is operated at its fundamental resonance frequency, therefore only the grating elements close to the edges of the metal structure, scatter surface waves into propagating bulk waves. Inside the grating, and far from the edges, BAWs are still excited by each individual grating element, but they interfere and cancel each other out, resulting in no propagation inside the bulk [101–103]. This is precisely what we observe in the Λ-filtered images, and in particular Fig. 3.6 (c) shows that when driving the short SAW cavity off-resonance, also the edges of the mirrors at the outer side of the cavity scatter BAWs since now the surface wave are not reflected and can travel through the mirrors.

In the same images, we observe high-amplitude points, appearing to be randomly distributed. These points, some of which are encircled as an example in Fig. 3.6 (c), correspond to particles on the GaAs surface or defects in the mirrors, which scatter surface

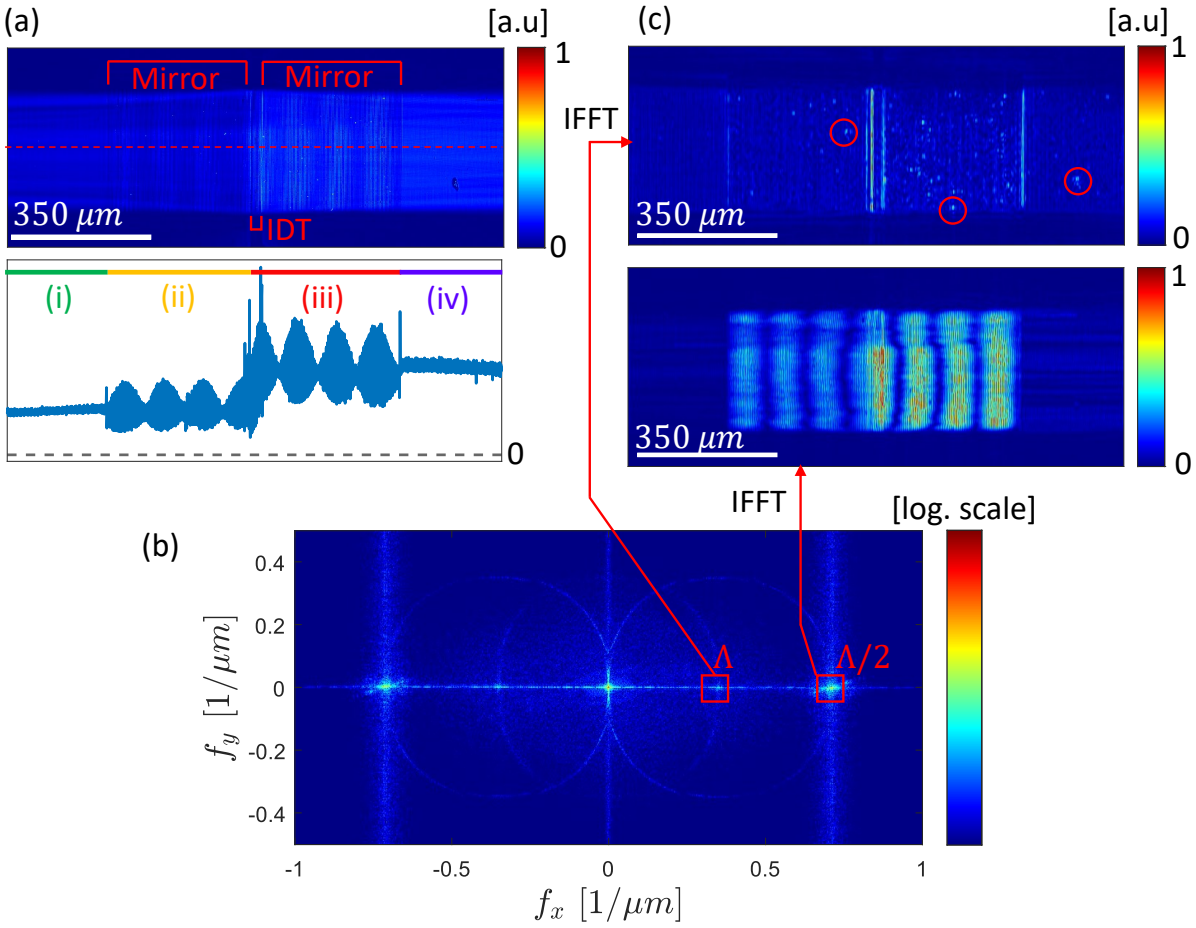

Figure 3.6: Acoustic field distribution in the short cavity, driven at a non-resonant frequency. (a) Amplitude of the out-of-plane displacement with a cross section of the acoustic field. The 4 regions (i) - (iv) highlight areas with different acoustic field distribution, and are discussed in the main text. (b) 2D Fourier transform of (a). (c) Fourier filtered images obtained from (b) by selecting only the Λ-term (top image) and the Λ/2-term (bottom image) in the Fourier spectrum.

waves, partially also into the bulk. Finally in the long cavity, and in the off-resonance measurement of the short cavity, we also observe a low-intensity Λ-periodic background, across the whole SAW cavity. We attribute this to BAWs originating from the surface scattering points mentioned above, propagating inside the bulk GaAs, and reflected from the bottom surface of the wafer. It is not fully clear why this background is not present in the short cavity, when driven at resonance.

For the short cavity driven off-resonance, we compare the 2D Fourier transform of the complex out-of-plane displacement, with the Fourier transform of the amplitude of the out-of-plane displacement, as shown in Fig. 3.7 (a) and (b). As explained in section II, the bulk waves correspond to a peak at zero spatial frequency in the Fourier transform of the complex displacement. Taking the amplitude of the displacement mixes the $f_x = 0$ periodicity of the bulk waves, with the $f_x = \pm 1/\Lambda$ periodicity of the left (right) traveling waves, effectively creating two sidebands in the displacement amplitude, as indicated by the red arrows in Fig. 3.7 (a) and (b). In Fig. 3.7 (c) we show the Fourier filtered displacement amplitude, obtained by selecting a small region around $f_x = 0$ in the Fourier

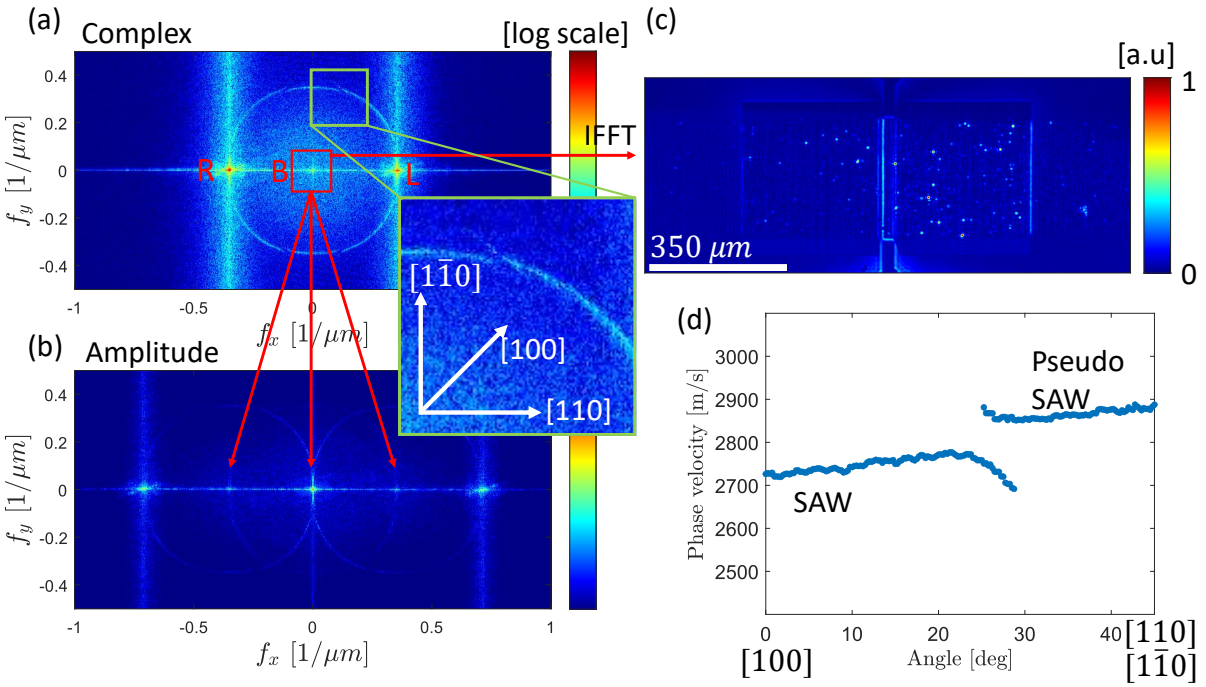

Figure 3.7: Comparison between Fourier transform of the complex displacement, and Fourier transform of the displacement amplitude, for the short cavity driven off-resonance. (a) Absolute value of the 2D Fourier transform of the complex displacement (amplitude and phase), with two peaks at the spatial frequencies $f_x = \pm 1/\Lambda$ corresponding to left and right traveling waves, and a peak at $f_x = 0$, corresponding to the bulk waves. (b) 2D Fourier transform of the amplitude of the displacement. We can see here a 'splitting' of the peaks corresponding to the bulk waves, as indicated by the red arrows. (c) Fourier filtered displacement amplitude, obtained from (a) by selecting only the spatial frequencies around $f_x = 0$. (d) Measured phase velocity as a function of the propagation angle, obtained from the Fourier transform in the inset of (a).

transform of the complex displacement. By comparison with the Filtered image obtained from the Fourier transform of the displacement amplitude, in Fig. 3.6 (c), we see that the two are equivalent, with only a difference in the intensities.

Finally we investigate the circular signal in the Fourier transform, as visible in the inset of Fig. 3.7 (a). We note that in the Fourier transform, the f_x axis in the Fourier transform correspond to the [110] direction and the f_y axis to the [1$\bar{1}$0] direction, but the two are equivalent due to the symmetry in the crystalline structure of GaAs. The direction at 45° from both the f_x and f_y axis is the [100] direction. The following analysis on the circular signal is done by considering the portion of the circle between the [100] and [1$\bar{1}$0] directions, because here the circular signal is clearly visible, as opposed to the [110] direction, where it is covered by the strong SAWs component that travels on the excitation axis. Due to the equivalence between the [1$\bar{1}$0] and [110] axis, in the following we will only refer to the [100] direction.

The circular signal in the Fourier transform corresponds to surface acoustic waves traveling off-axis with respect to the [110] direction along which the waves are excited. The presence of these off-axis propagating waves can be attributed partially to diffraction, and partially to scattering by impurities on the surface of the GaAs substrate.

By analyzing the circle, and converting it into an acoustic wavelength as a function of the angle of the propagating direction $\Lambda(\theta)$, we can calculate the phase velocity of the surface acoustic wave $v_{SAW}(\theta) = f_0 \times \Lambda(\theta)$, where $f_0 = 0.995\,\mathrm{GHz}$ is the excitation frequency. The result is shown in Fig. 3.7 (d), and shows the presence of two different kind of waves with different phase velocities, which branch out at an angle of about $25° - 30°$, from the [100] direction, which is at an angle of 45° from [110], the direction of excitation of the IDT transducer. The bottom branch is associated with a Rayleigh-type surface acoustic waves, while the top branch is a pseudo surface acoustic wave, which correspond to a Rayleigh wave coupled to a transverse horizontal bulk wave [106–108]. At the [110] direction the excited wave is a pure Rayleigh wave.

We note that in our measurement, the two branches stop at the branching point. The pure SAWs can in principle exist also at higher angles (measured from the [100] direction), but in our measurement are not detected due to their low amplitude. On the other hand, the pseudo SAW is not present at low angles, because the Rayleigh wave component disappears, leaving only the transverse horizontal bulk wave. The latter does not have an out-of-plane displacement component, and therefore is not directly detectable with our interferometer. Even if the amplitude of this transverse horizontal bulk wave is generally low, we hypothesize that the metal structures of the SAW cavity can partially scatter this wave into bulk waves with an out-of-plane component, and therefore be detected as a bulk wave in our interferometric measurements.

3.4 Conclusions and outlook

We have shown the power of analyzing spatial Fourier transforms of surface displacement in SAW devices. In particular we focused on the analysis of the acoustic fringes caused by interference of bulk and surface waves which, experimentally, only requires imaging the amplitude of the surface displacement, avoiding the technical complications of implementing phase detection at GHz frequencies.

Despite this method is only qualitative, since it can not measure the absolute amplitude of the bulk waves, it can be very useful in identifying the presence of unwanted bulk waves in surface acoustic wave devices, or equivalently unwanted surface waves in bulk acoustic wave devices. In SAW cavities, unwanted BAWs are scattered by edge discontinuities in the acoustic mirrors, creating losses in the surface acoustic wave cavity-mode. This is normally a secondary effect, since there are other loss mechanisms that are predominant, however it becomes important in high-Finesse SAW cavities where all other loss-mechanism are minimized, in particular if the cavity is operated at cryogenic temperatures.

This regime is of great importance for example in telecommunications and quantum technologies, and our novel method can potentially play an important role in reducing BAW losses in SAW cavities, increasing their finesse and providing better GHz electrical filters, or increasing the coupling between SAW phonons and quantum systems.